Ultrafast Pulse Retrieval from Partial FROG Traces Using Implicit Diffusion Models

Abhimanyu Borthakur, ^{1,*} Jack Hirschman, ^{2,3} and Sergio Carbajo ^{1,3,4,5}

¹Department of Electrical & Computer Engineering, UCLA, Los Angeles, CA 90095, USA

²Department of Applied Physics, Stanford University, Stanford, CA 94305, USA

³SLAC National Accelerator Laboratory, Menlo Park, CA 94025, USA

⁴Department of Physics and Astronomy, University of California Los Angeles, Los Angeles, CA 90095, USA

⁵California NanoSystems Institute, 570 Westwood Plaza, Los Angeles, CA 90095, USA

*abhimanyu911@ucla.edu

Abstract: Ultrashort laser pulses enable attosecond-scale measurements and drive breakthroughs across science and technology, but their routine use hinges on reliable pulse characterization. Frequency-Resolved Optical Gating (FROG) is a leading solution, forming a spectrogram by scanning the delay between two pulse replicas and recording the nonlinear signal spectrum. In online settings, however, dense delay-frequency scans are costly or impractical-especially for long pulses, wavelength regimes with limited spectrometer coverage (e.g., UV), or hardware with coarse resolution—yielding severely undersampled FROG traces. Existing reconstruction methods struggle in this regime: iterative algorithms are computationally heavy; convolutional networks blur fine structure; and sequence models are unstable when inputs are discontinuous or sparse. We present a generative diffusion framework tailored to recover ultrafast pulse intensity and phase from incomplete FROG measurements. Our model infers missing spectro-temporal content with high fidelity, enabling accurate retrieval from aggressively downsampled inputs. On a simulated benchmark of FROG-pulse pairs, the diffusion approach surpasses strong CNN and Seg2Seg baselines in accuracy and stability while remaining efficient enough for near-real-time deployment.

1. Introduction

Ultrashort laser pulses have revolutionized scientific research and technological applications over the past two decades. These pulses enable the study of ultrafast phenomena in physics, chemistry, and biology, providing unprecedented temporal resolution down to the attosecond scale [1,2]. The development of high-intensity, ultrashort laser pulses has been recognized with multiple Nobel Prizes, including the 2018 award for their chirped pulse amplification and the 2023 award for their contributions to extreme nonlinear optics and attophysics. Modern applications of ultrashort pulses span various fields, including precision machining, microscopy, medical imaging, and telecommunications [3–6]. Recent developments in spatial light modulation have further expanded the capabilities of ultrashort pulses, enabling tailored beam profiles for novel light-matter interactions. In practice, this meant new techniques had to be developed to characterize ultrashort pulses [7]. Among these innovations, Frequency-Resolved Optical Gating (FROG) emerged as a groundbreaking solution [8].

It accomplishes this through a self-referenced scheme in which the pulse is split into two replicas that overlap in a nonlinear medium, where one replica acts as a gate for the other. The spectrum of the nonlinear signal generated by their interaction is recorded while the relative delay between the replicas is scanned. The resulting two-dimensional map of intensity versus frequency and delay is effectively a spectrogram of the pulse and is known as the FROG trace [9].

For online operation or control systems, time delay scans can be prohibitively expensive for long pulses (therefore, creating a bottleneck for data collection) or limited by spectrometer resolution [10].

Even if high-resolution spectrometers are deployed, they might not be appropriate for a particular wavelength of light, such as UV, where short bandwidth pulses yield only a few sample points [11,12]. This motivates the need for a new modeling framework that can democratize access to FROG technologies for stakeholders limited by the aforementioned constraints. Automated pulse reconstruction from incomplete (or partial) FROG traces is therefore an increasingly valuable pursuit. Here, 'incomplete' designates any FROG trace in which the two-dimensional delay–frequency grid is extensively undersampled, for example, retrieving a 512-point pulse array from an aggressively downsampled 64 x 64 two-dimensional trace, instead of the full 512 x 512 trace.

Traditional iterative FROG reconstruction is computationally intensive, limiting its use in large-scale simulations. Recently, convolutional neural networks (CNNs) and sequence-to-sequence (Seq2Seq) models have shown great promise in retrieving ultrafast pulse intensity and phase from FROG spectrograms, achieving much faster reconstructions than traditional iterative algorithms [10,13]. However, these deep learning methods struggle with downsampled FROG traces: CNNs cannot effectively model temporal context, and Seq2Seq models struggle with incomplete data [14–16]. Specifically, CNNs aggregate information through stacked local filters, which can lead to blurring or averaging of fine input details [17]. Further, CNNs that excel on dense measurements misfire on sparse ones [18]. Seq2Seq or sequential models, by contrast, process their inputs sequentially and therefore assume a continuous input stream. Discontinuities such as those between the pixels in partial FROG traces, hence, break the hidden-state continuity and allow vanishing-gradient or exploding-gradient pathologies to dominate, leading to unstable optimization updates [19].

We introduce a novel generative diffusion model that can model (missing) spectro-temporal information with high fidelity to comprehensively address the limitations of and outcompete previous SOTA ML techniques, marking an original stride in robust retrieval of ultrafast pulses from sparse input spaces. We compare our diffusion approach with other techniques by benchmarking them on a simulated dataset of FROG-pulse pairs. While this study is broadly applicable to FROGs and other spectrogram-based techniques, we focus our attention on Second Harmonic Generation (SHG) FROGs for brevity.

2. Methods

2.1. Data generation

We generate synthetic data by simulating sinc-shaped ultrashort pulses modulated by linear chirp, self-phase modulation (SPM), and third-order phase terms. Each pulse is a 256-point array over a 100 fs window, modeled using Eq. 1, with the amplitude A(t) given by Eq. 2 and the phase $\Phi(t)$ represented by Eq. 3. This E(t) is our ground truth pulse and the full SHG FROG trace is computed as the squared magnitude of the Fourier transform of the product E(t)E(t – τ), and downsampled 8x (on both axes) to produce a 32 × 32 spectrogram $I(\omega, \tau)$. We generate 22,000 samples, varying $t_{\text{FWHM}} \in [20, 29]$ fs, $a_{\text{chirp}} \in [0.01, 0.02]$ fs², $b_{\text{SPM}} \in [5,8.9]$ W⁻¹, and c3 $\in [10^{-4},4 \times 10^{-4}]$ fs⁻³. The dataset is split into 18,000 training, 2,000 validation, and 2,000 test tuples, each of the form ($I(\omega, t)$, (A(t), $\Phi(t)$)), with traces normalized to unit peak intensity through division by the maximum value.

E(t) = A(t) exp[i
$$\Phi$$
(t)] (Eq.1)
A(t) = |sinc(t/t_{FWHM})| (Eq. 2)
 Φ (t) = $a_{chirp}t^2 + b_{SPM}|A(t)|^2 + c_3t^3$ (Eq. 3)

2.2. Machine Learning (ML) Modeling and Pulse Reconstruction

The goal of our trained ML models is to recover A(t) and $\Phi(t)$ from an unseen (test set) I(ω , τ) as input. We compare three architectures for SHG-FROG pulse reconstruction: a Visual Geometry Group (VGG) CNN, a Seq2Seq model with attention, and a diffusion model. The VGG network [20] serves as a CNN baseline due to its simplicity and strong performance in image-based tasks. The Seq2Seq model [10] demonstrated state-of-the-art accuracy on partial SHG-FROG traces, outperforming classical iterative algorithms [21,22]. Our diffusion model integrates a CNN encoder with a sequence model to capture both spatial and temporal structure and is trained using the Denoising Diffusion Implicit Model (DDIM) framework [23]. A snapshot of the three models is provided in Figure 1. For the sake of completeness, we also benchmark the performance on other models, including CapsNet [24], ResNet [25], and DenseNet [26]. All models are implemented in PyTorch.

2.3. Diffusion model specifics

Our diffusion model is trained using Algorithm 1. It uses two neural networks $f_{\mathbf{w}}$ (for amplitude) and $g_{\mathbf{w}}$ (for phase), which share a common encoder (see Figure 1) for the input spectrogram I. Each training iteration begins by sampling a diffusion timestep t using a learned sampler network $\operatorname{Sampler}_{\theta}(I)$. This sampler outputs a categorical distribution over t (of total T diffusion steps), and a Gumbel-Softmax method is used to sample t in a differentiable way [27]. By learning the sampling policy for t, the training focuses on more informative noise levels instead of uniformly sampling timesteps, similar in spirit to recent non-uniform timestep scheduling strategies that accelerate diffusion model training [28]. Given the chosen t, the algorithm diffuses forward: it adds Gaussian noise $\epsilon \sim \mathcal{N}(0,I)$ to the ground-truth amplitude A to produce a noisy amplitude $x_t = \sqrt{\alpha_t}A + \sqrt{1-\alpha_t}\epsilon$. Here $\alpha_t = \prod_{\tau=1}^t (1-\beta_\tau)$ corresponds to a standard forward diffusion process with variance schedule β_t – in this case a cosine noise schedule that smoothly varies noise intensity across T=1000 steps [29]. The amplitude network $f_{\rm w}$ then tries to denoise this sample: it takes as input the noisy x_t , the spectrogram I, and the time index t (passed through a sinusoidal time embedding), and predicts \hat{x}_0 an estimate of the original clean amplitude. Subsequently, the phase network $g_{\mathbf{w}}$ aims to predict the spectral phase: it uses the same encoded features of I along with the amplitude information to output $\hat{\Phi}$, an estimate of the true phase Φ . During training $g_{\mathbf{w}}$ is given the ground-truth A as input, whereas at test time, it would use $f_{\mathbf{w}}$'s predicted amplitude. The two networks are trained in succession, and the Adam optimizer [30] is used to update their parameters as well as the weights of the sampler network. The training loop repeats for 100 epochs, and throughout training, the learning rates are gradually annealed with a cosine schedule [31] from a starting value of 10^{-4} .

Importantly, both $f_{\rm W}$ and $g_{\rm W}$ rely on the same encoder architecture to extract a 1024-dimensional feature representation z from the input spectrogram I. A more detailed argument for the design choice is detailed in our Supplement 1. Specifically, this shared encoder first applies a Squeeze-and-Excitation (SE) ResNet backbone – a convolutional network with SE blocks that adaptively recalibrate channel-wise feature responses [32] – to process the 32×32 FROG trace into spatial feature maps. These feature maps (of shape $4 \times 4 \times 128$ after the ResNet layers) are then flattened into a sequence of length 16 and fed into a bidirectional Long Short-Term Memory (LSTM) network to capture global structure across the image [33]. The LSTM's output (a sequence of 16 vectors) is next aggregated by an additive attention mechanism wherein the model learns to weight and sum the LSTM outputs into a single context vector (1024-d) that represents the salient information in the spectrogram. This encoding design is shared between the two tasks – for amplitude prediction, the context vector is concatenated with the noisy amplitude x_t and the time embedding before being passed through $f_{\rm W}$'s fully-connected layers to predict \hat{x}_0 , while for phase prediction, the context vector is concatenated with the amplitude vector and fed into $g_{\rm W}$'s MLP to produce $\hat{\Phi}$.

Our inference procedure in Algorithm 2 (see Figure 2) follows the DDIM sampling [23] algorithm where the S timesteps are sampled through our learned sampler. For our experiments, we set S=10. The inference algorithm is illustrated in Figure 2.

3. Results and Discussion

From Table 1, it is clear that the diffusion model outperforms every other model in terms of average amplitude and phase reconstruction error. The VGG and the Seq2Seq models are the second- and third-best-performing models, respectively, in terms of amplitude mean absolute error. We can observe the reconstructions of each of the top 3 models on FROG instances randomly sampled from across their error distributions in Figure 3. The amplitude reconstruction of our VGG CNN is noisy and consists of local artifacts because the strictly local convolutional receptive fields overestimate pixel-level variations.

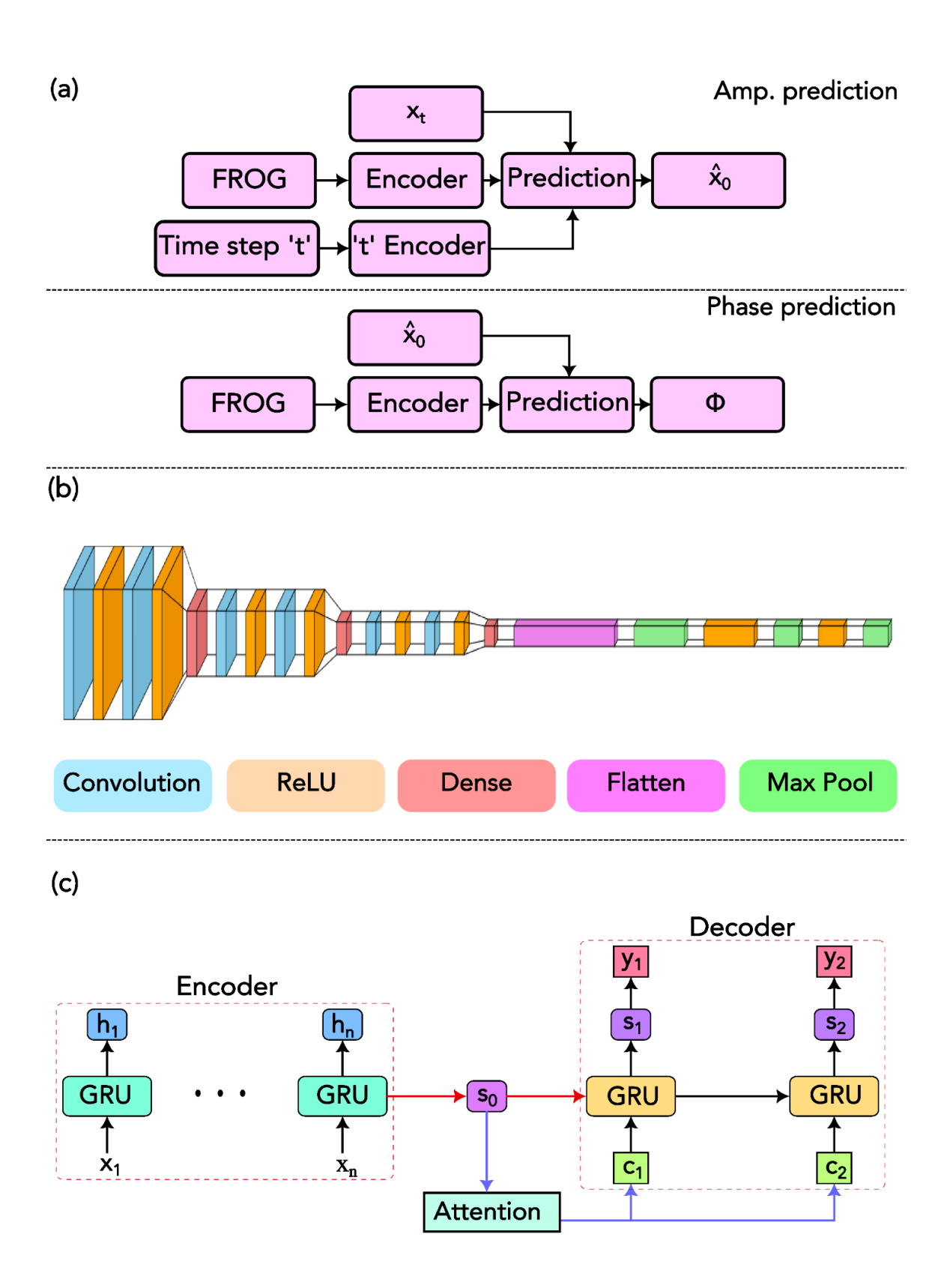


Fig. 1. (a) Diffusion denoiser (b) VGG CNN (c) Seq2Seq network

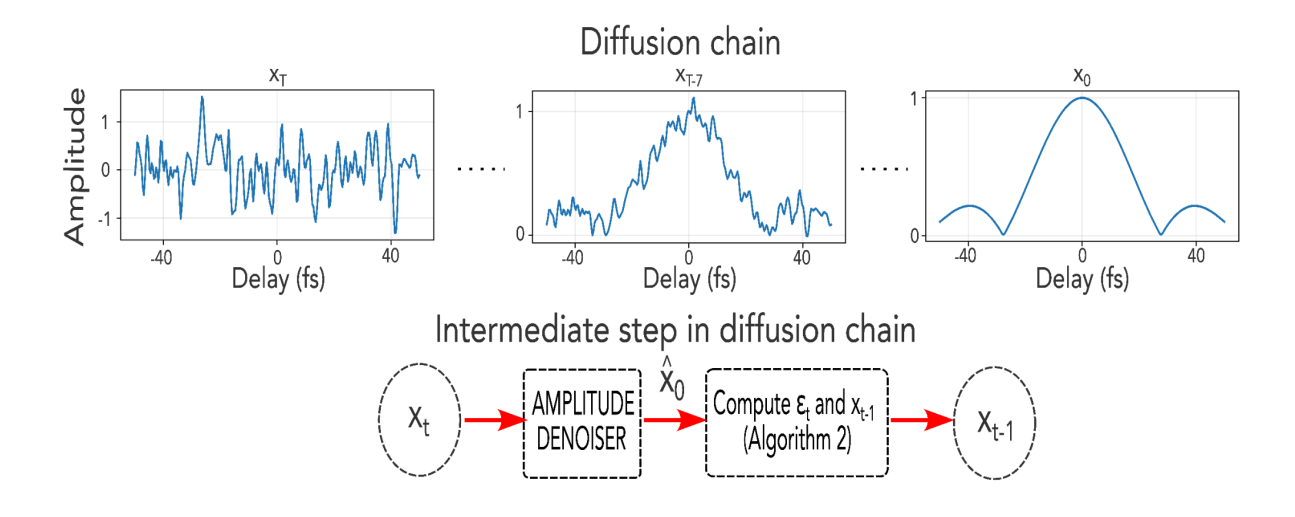


Fig. 2. High-level visualization of Algorithm 2

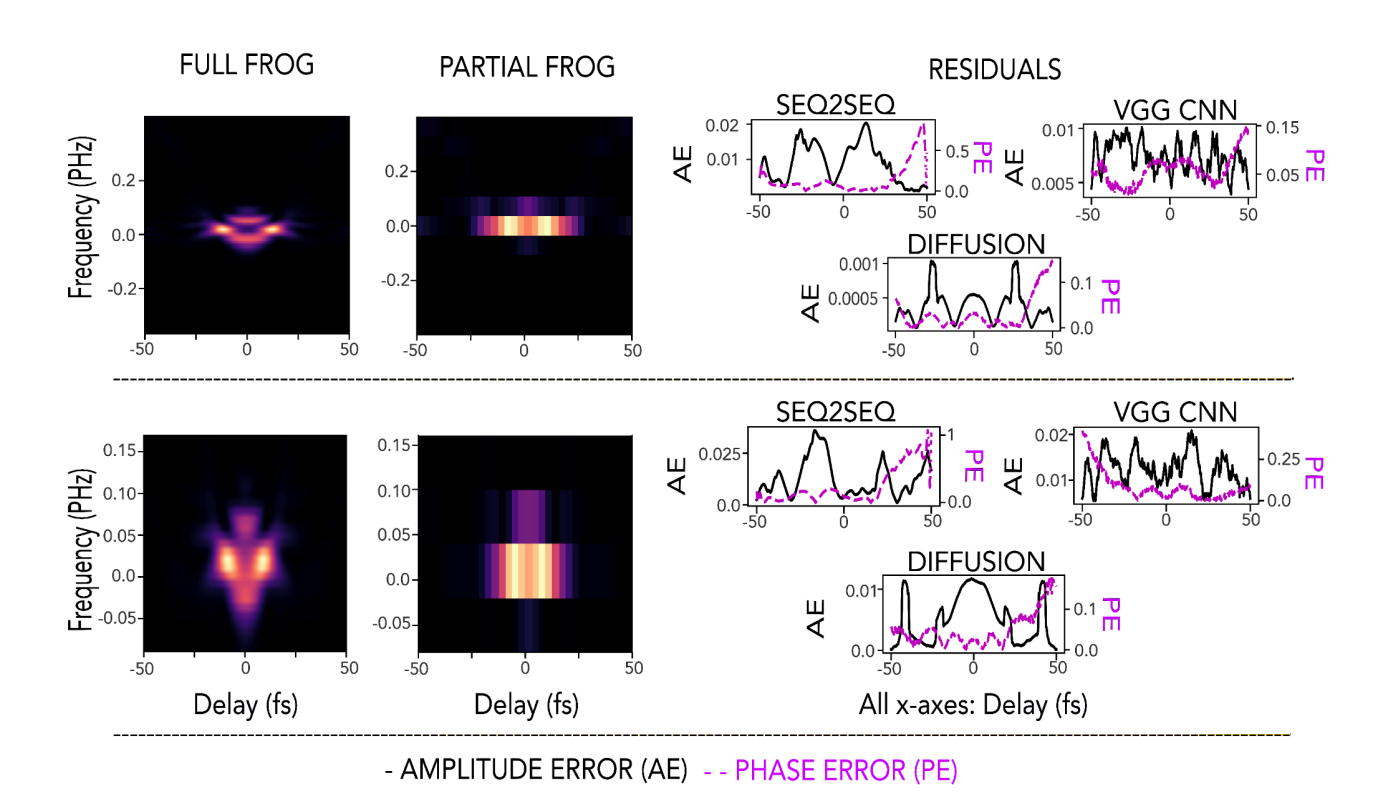


Fig. 3. Pulse reconstruction residuals for VGG, Seq2Seq and diffusion on FROG traces sampled from 25th (top) and 50th (bottom) percentiles of the error distribution (on test set). Individual sample reconstruction errors for each model are listed in Table 2.

```
Algorithm 1: Training the Implicit Diffusion Model
```

```
Input: Training set \mathscr{D} = \{(I_n, A_n, \Phi_n)\}, noise schedule \{\beta_t\}_{t=1}^T, epochs E, batch size B, learning rates
Output: Model parameters w, sampler parameters \theta
for t \leftarrow 1 to T do
 \alpha_t \leftarrow \prod_{\tau=1}^t (1-\beta_{\tau});
repeat
      Shuffle \mathcal{D} into batches of size B;
      foreach batch (I, A, \Phi) do
             // 1) sample timestep via learned sampler
             \ell \leftarrow \operatorname{Sampler}_{\theta}(I);
             t \leftarrow \operatorname{arg\,max} \operatorname{GumbelSoftmax}(\ell);
             // 2) diffuse forward
             \varepsilon \sim \mathcal{N}(0,I);
             x_t \leftarrow \sqrt{\alpha_t} A + \sqrt{1 - \alpha_t} \varepsilon;
             // 3) predict and compute losses
             \hat{x}_0 \leftarrow f_{\mathbf{w}}(A_t, I, t);
             \mathscr{L}_A \leftarrow \|\hat{x}_0 - A\|_1;
             \hat{\Phi} \leftarrow g_{\mathbf{w}}(I,A);
             \mathscr{L}_P \leftarrow \|\hat{\Phi} - \Phi\|_1;
             // 4) update model & sampler
             \{\mathbf{w}, \boldsymbol{\theta}\} \leftarrow \operatorname{Adam}(\mathscr{L}_A, \mathscr{L}_P; \boldsymbol{\eta}_{amp}, \boldsymbol{\eta}_{ph}, \boldsymbol{\eta}_{sam})
until epoch > E or convergence;
return \mathbf{w}, \boldsymbol{\theta}
```

Algorithm 2: Inference

```
Input: Test trace I, trained models g_{\mathbf{w}}, f_{\mathbf{w}}, sampler \boldsymbol{\theta}, substeps S
Output: Reconstruction (\hat{A}, \hat{\Phi})
x \sim \mathcal{N}(0, I);
T \leftarrow \text{diff\_steps} - 1;
\ell \leftarrow \operatorname{Sampler}_{\theta}(I);
\{t_i\}_{i=2}^S \leftarrow \arg\max^{S-1} (GumbelSoftmax(\ell));
t_1 \leftarrow T; sort \{t_i\}_{i=1}^S in descending order;
for i \leftarrow 1 to S do
      \hat{A}_0 \leftarrow f_{\mathbf{w}}(x, I, t_i);
      \varepsilon \leftarrow (x - \sqrt{\alpha_{t_i}} \hat{A}_0) / \sqrt{1 - \alpha_{t_i}};
      if i < S then
            x \leftarrow \sqrt{\alpha_{l_{i+1}}} \hat{A}_0 + \sqrt{1 - \alpha_{l_{i+1}}} \varepsilon;
      else
        // final refinement
\hat{A} \leftarrow x;
\hat{\Phi} \leftarrow g_{\mathbf{w}}(I,\hat{A});
return \hat{A}, \hat{\Phi};
```

Table 1. Mean Absolute Error (MAE) for each model averaged on the test set

Model	Amp MAE	Phase MAE	
Seq2Seq [10]	0.01256	0.29125	
VGG [20]	0.00941	0.10170	
Diffusion (this work)	0.00070	0.05375	
CapsNet [24]	0.01816	0.13267	
ResNet [25]	0.03361	0.20523	
DenseNet [26]	0.02405	0.18485	

Table 2. Reconstruction errors for illustrative examples in Figure 3

Percentile index	Seq2Seq		VGG		Diffusion	
	Amp MAE	Phase MAE	Amp MAE	Phase MAE	Amp MAE	Phase MAE
25	0.0089	0.1412	0.0075	0.0585	0.0004	0.0304
50	0.0130	0.2429	0.0125	0.0847	0.0006	0.0458

The amplitude reconstruction of the Seq2Seq, however, is smoother but less accurate as the recurrent attention operation averages information across neighbouring time-steps, suppressing noise while introducing a smoothing bias. While both CNN and Seq2Seq produce visually appealing results for the phase, it is clear, from Figure 3 and Table 1, that the diffusion does best, both visually and on average. The mean inference (prediction) time of the diffusion model is 0.052 seconds per sample (batch size = 1) on a Google Colab A100 GPU.

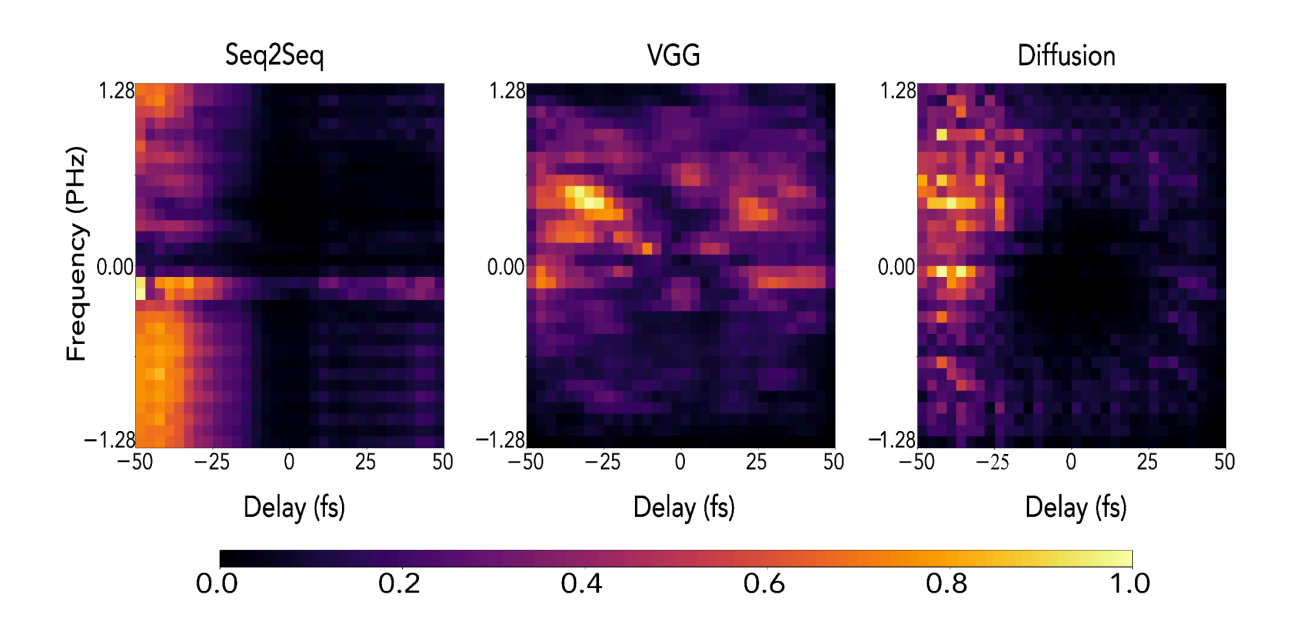


Fig. 4. Average saliency maps obtained on the test set

The aforementioned behaviour of each model can be analysed quantitatively and qualitatively from the average saliency maps (see Figure 4) obtained on the unseen test split. These maps are built as follows: for every test set trace, we back-propagate the mean absolute error on both amplitude and phase, take the absolute input gradients of this error with respect to the 2D trace, normalize the two maps separately, fuse them with an equal-weight summation, and finally average the result over the entire test set. A bright response at any region of the map indicates that the respective network is making strong use of that region for predictions and vice versa.

The diffusion model exhibits an almost radially symmetric, low-contrast pattern with a broad annulus before tapering into subtle high-frequency streaks. This confirms that the diffusion network first distributes responsibility evenly across the trace, capturing the global pulse shape before sharpening its attention on the highest-frequency fringes to polish residual error. The convolutional VGG regressor, in contrast, lights up only a few bright blotches scattered around mid-band delays and frequencies. Since it fixates on just these local motifs and largely ignores the rest of the grid, its reconstructions end up patchy and noisy wherever those cues are missing. The Seq-to-Seq with Bahdanau attention concentrates almost all gradient mass along a single vertical strip of delays and selective horizontal slices in frequency. The recurrent attention, therefore, latches onto a few selective anchor points, propagates information temporally, and consequently outputs a smoother, yet biased reconstruction.

4. Conclusion

We have presented a novel generative diffusion model capable of reconstructing ultrashort pulses from partial FROG traces with high fidelity. This model outperforms both traditional deep learning approaches, such as CNNs, as well as the current state of the art (Seq2Seq) in this domain. CNNs are great at exploiting local patterns in input data to make predictions; however, they struggle to model long-term spectro-temporal relationships when the input is aggressively downsampled. Sequential networks augmented with attention (like Seq2Seq) are better at modeling such dependencies but produce biased estimates on incomplete inputs. These limitations are corroborated by the performance of these models on the unseen test set and the resulting saliency maps.

The diffusion model addresses these limitations by denoising a noisy latent vector to obtain the reconstructions with the FROGs acting as an additional mode of context rather than the sole input.

This accurate and rapid reconstruction algorithm marks a novel stride in generative pulse retrieval for highly incomplete spectrograms, bridging the gap between physical interpretability and data-driven inference. Beyond outperforming existing models, our diffusion-based framework opens a path toward real-time, high-fidelity diagnostics of ultrashort pulses even in scenarios constrained by limited temporal or spectral resolution. Such capability has broad implications: experimental setups that cannot afford high-end detectors or delay lines can now recover full pulse information from sparse measurements; university and teaching labs can achieve state-of-the-art characterization with affordable equipment; and industrial or facility-scale systems can leverage the model for online feedback, adaptive control, and stability optimization during live operation [34–37]. By transforming partial measurements into reliable reconstructions, this work pushes FROG retrieval into a new generative regime—one that democratizes ultrafast pulse characterization and extends its reach from controlled laboratory conditions to resource-limited, high-throughput, and in situ environments.

Acknowledgements

This work has been supported by the following grants: DOE DE-FOA-0002859, DOE DE-AC02-76SF00515, NSF 2436343, ONR N00014-24-1-2038

References

- 1. F. Krausz and M. Ivanov, "Attosecond physics," Rev. Mod. Phys. 81, 163–234 (2009).
- 2. F. Calegari and F. Martin, "Open questions in attochemistry," Commun. Chem. 6, 184 (2023).
- 3. W. Sibbett, A. A. Lagatsky, and C. T. A. Brown, "The development and application of femtosecond laser systems," Opt. Express **20**, 6989–7001 (2012).
- 4. K. Sugioka and Y. Cheng, "Ultrafast lasers—reliable tools for advanced materials processing," Light Sci. Appl. 3, e149–e149 (2014).
- 5. C. Xu and F. W. Wise, "Recent advances in fiber lasers for nonlinear microscopy," Nat. Photonics 7, 875–882 (2013).
- 6. W. H. Knox, "Ultrafast technology in telecommunications," IEEE J. Sel. Top. Quantum Electron. 6, 1273–1278 (2000).
- T. Wong and R. Trebino, "Recent developments in experimental techniques for measuring two pulses simultaneously," Appl. Sci. (Basel) 3, 299–313 (2013).
- 8. R. Trebino, Z. Guang, P. Zhu, and M. Rhodes, "The measurement of ultrashort laser pulses," in 2018 2nd URSI Atlantic Radio Science Meeting (AT-RASC) (IEEE, 2018).
- 9. R. Trebino and D. J. Kane, "Using phase retrieval to measure the intensity and phase of ultrashort pulses: frequency-resolved optical gating," J. Opt. Soc. Am. A Opt. Image Sci. Vis. **10**, 1101 (1993).
- Y. Zeng, Z. He, X. Guo, G. Zhu, and X. Zhu, "Deep learning reconstruction algorithm for frequency-resolved optical gating," Opt. Lett. 49, 3741–3744 (2024).
- 11. R. Lemons, J. Hirschman, H. Zhang, C. Durfee, and S. Carbajo, "Nonlinear shaping in the picosecond gap," arXiv [physics.optics] (2024).
- 12. R. Lemons, N. Neveu, J. Duris, A. Marinelli, C. Durfee, and S. Carbajo, "Temporal shaping of narrow-band picosecond pulses via noncolinear sum-frequency mixing of dispersion-controlled pulses," Phys. Rev. Accel. Beams 25, (2022).
- 13. T. Zahavy, A. Dikopoltsev, D. Moss, G. I. Haham, O. Cohen, S. Mannor, and M. Segev, "Deep learning reconstruction of ultrashort pulses," Optica 5, 666 (2018).
- 14. V. Antun, F. Renna, C. Poon, B. Adcock, and A. C. Hansen, "On instabilities of deep learning in image reconstruction and the potential costs of AI," Proc. Natl. Acad. Sci. U. S. A. **117**, 30088–30095 (2020).
- 15. M. Waqas and U. W. Humphries, "A critical review of RNN and LSTM variants in hydrological time series predictions," MethodsX 13, 102946 (2024).
- 16. X. Wang, R. Girshick, A. Gupta, and K. He, "Non-local Neural Networks," in 2018 IEEE/CVF Conference on Computer Vision and Pattern Recognition (IEEE, 2018).
- 17. C. Ledig, L. Theis, F. Huszar, J. Caballero, A. Cunningham, A. Acosta, A. Aitken, A. Tejani, J. Totz, Z. Wang, and W. Shi, "Photo-realistic single image super-resolution using a generative adversarial network," in 2017 IEEE Conference on Computer Vision and Pattern Recognition (CVPR) (IEEE, 2017).
- 18. E. Y. Sidky, I. Lorente, J. G. Brankov, and X. Pan, "Do CNNs solve the CT inverse problem?," IEEE Trans. Biomed. Eng. **68**, 1799–1810 (2021).
- 19. J. Kim, H. Kim, H. Kim, D. Lee, and S. Yoon, "A comprehensive survey of deep learning for time series forecasting: architectural diversity and open challenges," Artif. Intell. Rev. **58**, (2025).
- 20. K. Simonyan and A. Zisserman, "Very deep convolutional networks for large-scale image recognition," arXiv [cs.CV] (2014).
- 21. D. J. Kane, "Real-time measurement of ultrashort laser pulses using principal component generalized projections," IEEE J. Sel. Top. Quantum Electron. 4, 278–284 (1998).
- 22. J. R. Fienup, "Phase retrieval algorithms: a comparison," Appl. Opt. 21, 2758-2769 (1982).
- 23. J. Song, C. Meng, and S. Ermon, "Denoising Diffusion Implicit Models," arXiv [cs.LG] (2020).
- 24. Y. Zhu, Z. Zhang, R. Zhang, and L. Zhou, "SinBasis Networks: Matrix-Equivalent Feature Extraction for Wave-Like Optical Spectrograms," arXiv [cs.LG] (2025).
- 25. X. Dong and X. Wei, "Two-step hybrid retrieval algorithm for characterizing ultrashort optical pulse from its SHG-FROG trace," Opt. Commun. **587**, 131940 (2025).
- 26. I. Tóth, A. M. M. Gherman, K. Kovács, W. Cho, H. Yun, and V. Toşa, "Reconstruction of femtosecond laser pulses from FROG traces by convolutional neural networks," Photonics **10**, 1195 (2023).
- 27. E. Jang, S. Gu, and B. Poole, "Categorical Reparameterization with Gumbel-Softmax," arXiv [stat.ML] (2016).

- 28. T. Zheng, P.-T. Jiang, B. Wan, H. Zhang, J. Chen, J. Wang, and B. Li, "Beta-tuned timestep diffusion model," in Lecture Notes in Computer Science, Lecture Notes in Computer Science (Springer Nature Switzerland, 2025), pp. 114-130.
- 29. A. Nichol and P. Dhariwal, "Improved denoising diffusion probabilistic models," arXiv [cs.LG] (2021).
- 30. D. P. Kingma and J. Ba, "Adam: A method for stochastic optimization," arXiv [cs.LG] (2014).
- 31. I. Loshchilov and F. Hutter, "SGDR: Stochastic gradient descent with warm restarts," arXiv [cs.LG] (2016).
 32. J. Hu, L. Shen, and G. Sun, "Squeeze-and-Excitation Networks," in 2018 IEEE/CVF Conference on Computer Vision and Pattern Recognition (IEEE, 2018).
- 33. S. Hochreiter and J. Schmidhuber, "Long short-term memory," Neural Comput. 9, 1735–1780 (1997).
- 34. J. Hirschman, R. Lemons, M. Wang, P. Kroetz, and S. Carbajo, "Design, tuning, and blackbox optimization of laser systems," Opt. Express 32, 15610-15622 (2024).
- 35. J. Hirschman, E. Abedi, M. Wang, H. Zhang, A. Borthakur, J. Baker, and S. Carbajo, "Long-short term memory model for χ² nonlinear processes: Enhancing simulation with ML," arXiv [physics.optics] (2025).
- 36. J. E. Hirschman, E. Abedi, H. Zhang, R. Lemons, A. Borthakur, J. Baker, and S. Carbajo, "Towards digital twins of high-power laser systems," in Solid State Lasers XXXIV: Technology and Devices, W. A. Clarkson and R. K. Shori, eds. (SPIE, 2025), p. 50.
- 37. J. Hirschman, A. Borthakur, H. Zhang, E. Abedi, J. Baker, R. Lemons, and S. Carbajo, "Machine Learning Optimization of Nonlinear Dynamics in High-Power Laser Systems Using Digital Twins," SS149_5 (2025).